Originally Published with ECS 2022: Proceedings from the 242nd Electrochemical Society Meeting

Emerging Technologies for Advanced 3D Package Characterization to Enable the More-than-Moore Era

Seeing beyond

C. Hartfield, W. Harris, A. Gu, and M. Terada
Carl Zeiss Microscopy LLC, 5300 Central Parkway, Dublin, California, 94568, USA

V. Viswanathan and L. Jiao
Research Microscopy Solutions Carl Zeiss Pte Ltd, 80 Bendemeer Road, #10-01, 339949 Singapore

T. Rodgers
Carl Zeiss Microscopy GmbH, Carl-Zeiss-Straße 22, 73447, Oberkochen, Germany

Abstract

The line between packaging and silicon interconnect technology is blurring due to a reduction in package interconnect dimensions, which drives an increase in image resolution requirements. It is becoming more difficult to localize and image defects and structures throughout the packaging life cycle, from materials selection, through package and silicon design co-optimization, development, production, and field failure diagnostics. Characterization and failure analysis (FA) solutions must provide fast results for rapid development of packages meeting the required electrical, mechanical and reliability specifications with high yield and quality. Heterogeneous integration and complex packages containing multiple die drive new approaches to rapidly characterize structures, defects and processes. This paper presents new artificial intelligence (AI) developments in 3D X-ray microscopy (XRM) for non-destructive submicron-resolution imaging of packages. It also introduces the latest developments in focused ion beam (FIB) microscopes adapted with an integrated fs-laser for precise and fast analysis of deeply buried features in advanced packages.

Introduction

In the past, the main function of a semiconductor package was to protect the integrated circuit while providing a way to move the signals into a printed circuit board. In recent years, the package has evolved into a critical component providing dense off-chip integration for highest system performance and the extension of Moore's Law. There is a requirement in advanced packaging for 3D interconnects at fine pitch and high density (Figure 1). This is driven by the heterogeneous integration required for high performance computing and mobile devices across a vast array of industries, including IOT, 5G, AI, RF/analog, and automotive. Package interconnect scaling has crossed over into interconnect dimensions formerly only found within die-level BEOL circuitry. Microbumps in 3D packages are 8,000 times smaller than solder balls, and 124 times smaller than C4 bumps, while package I/O pitch is approaching 1 µm [1].

Package designs become 3D by adding more layers, decreasing layer thicknesses, and stacking die. Advanced 3D packages are also incorporating the latest silicon technologies. At the die level, there are efforts to develop backside power delivery networks to address the resistance issues that arise from scaling [2]. As both sides of the die are metallized, even more challenges are introduced to isolate faults and access a buried region of interest, characterize structures and regions of interest in 3D, collect sufficient data, and perform FA without creating artifacts or missing or destroying the region of interest. New advancements in 3D XRM for non-destructive imaging and FIB microscopes for package-level sample preparation bring significant capabilities to package characterization and physical failure analysis.

Advanced Microscopy Innovations For 3D Package Analysis

New packages are developed through a series of learning cycles to enable material selection, design and co-optimization with silicon-level processes, development of multiprobe test technologies, and final products meeting performance and reliability specifications. The push and pull dance between package characterization capability and emerging package technology requirements has existed since the package was first invented. X-ray inspection is one of the oldest package analysis techniques, and C-mode scanning acoustic microscopy (C-SAM) became widespread after the 1980's due to industry adoption of JEDEC standards addressing "popcorn cracking" defects in moisture-sensitive packages [4]. C-SAM has been challenged by the increasing numbers of thin layers and die stacking in 3D packages, and its application has become limited, driving research into GHz techniques [4, 5]. This leads to stronger reliance on X-ray imaging for non-destructive package analysis.

As X-ray inspection has moved from 2D to 3D, the analysis time has increased. To enable 3D data at a suitable intersection of resolution and throughput, different types of 3D X-ray techniques have evolved. These include microcomputed tomography (microCT), X-ray laminography (sometimes called 2.5D X-ray), and X-ray microscopy (XRM), which are described later in this paper.

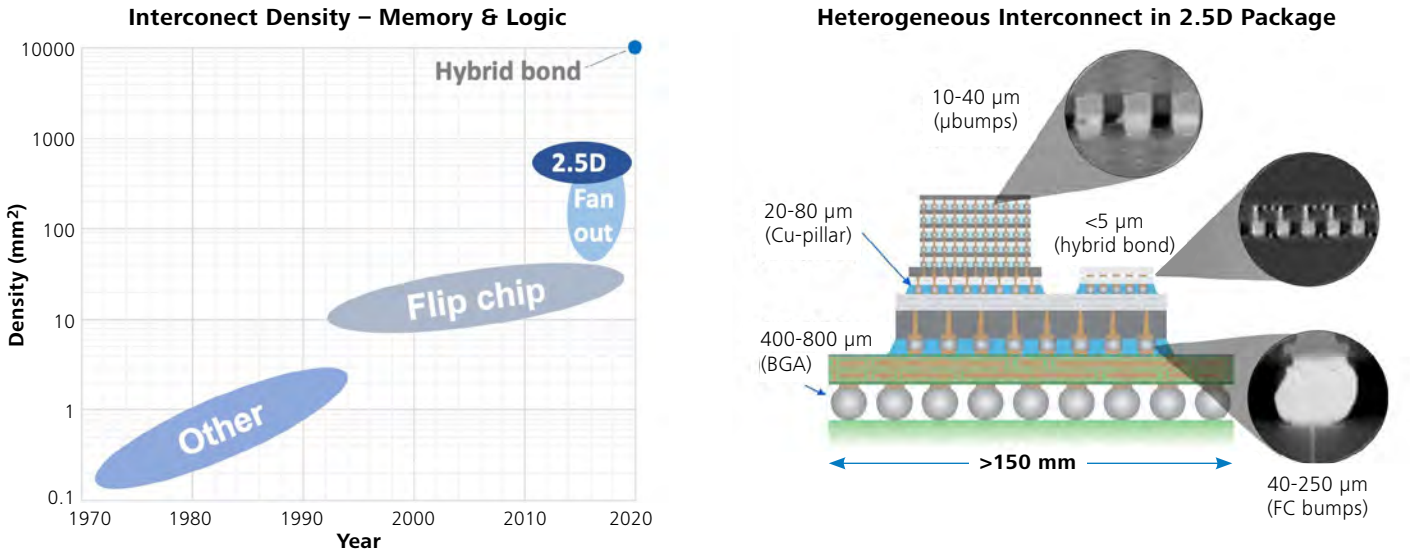

Figure 1 *The density of package interconnect has accelerated in recent years [3] and now approaches 1 µm pitch, with highest densities occurring in hybrid bond technology (left). Interconnects of different types and pitches co-exist in 2.5/3D packages, some of which can be ≥150 mm diameter or larger (right). The zoomed views are virtual slices of 3D XRM data (not shown to scale).*

When it comes to destructive physical failure analysis (PFA), the requirement for artifact-free cross sections of packages and their fast-shrinking structures drives the use of ion beam technologies. This includes broad ion beams (BIB), which are typically Ar, and plasma focused ion beams (PFIB), typically Xe. Advances in packaging technology are pushing BIB and PFIB beyond their limits, due to the combined need for precise end-pointing and rapid site-specific removal of millimeter volumes of material. Broad ion beams can be applied to large areas but lack the end-pointing specificity required by today's advanced fine-pitch high density interconnect. While the traditional Ga FIB and Xe PFIB typically used for semiconductor analysis allow end-pointing on the nanometer scale, both are unable to deliver the milling rates needed for rapid site-specific cross-sectional analysis of structures deeply buried within heterogeneous 2.5/3D and SiP packages.

Advances in 3D X-ray Imaging

Introduction to 3D X-ray Imaging Techniques

X-ray imaging is a transmission microscopy technique, and the composition and size of the sample affect parameters such as scan time, achievable resolution, contrast, and the interplay amongst these variables. To acquire a 3D X-ray image, a sample is placed between an X-ray source and a detector. The sample is automatically rotated to different angular positions, and projection images are collected at the different angles before being reconstructed into a 3D image. For microCT, a flat-panel detector is used, and principles of geometric magnification mandate placing the sample as close as it can get to the source to achieve the highest magnification (Figure 2a). If the magnification becomes limited by a sample size that requires a longer working distance, then resolution will also be limited as a function of the sample size. Often in microCT, the sample must be cut to a small size to enable the highest-resolution imaging. Semiconductor package dimensions can range from <1 mm on a side up to >150 mm, and advanced packages use wafer-level packaging. To enable 3D X-ray imaging at submicron resolution on large samples, 3D XRM was introduced (Figure 2b). It has a geometric magnification component, and it also incorporates optical magnification by implementing scintillator-coupled objective lenses as detectors. Optical magnification enables high magnification and therefore high resolution when the sample is far away from the source, regardless of the sample size (Figure 2c). In the example shown in Figure 2c, a comparison of microCT and XRM results is shown for a package approximately 40 mm in diameter. While microCT delivers poor resolution for this large sample size, XRM with optical magnification can still resolve fine details within the structure.

X-ray laminography is an X-ray imaging method that emerged to scan packages and printed circuit boards fast at relatively low resolutions. It has a configuration that allows scanning a high aspect ratio sample by passing the beam only through the short axis and avoiding the long axis. This is shown in Figure 3a, where the X-ray beam always takes a short path through the package. This scanning strategy unfortunately causes streak artifacts in the non-planar views when the images are reconstructed (Figure 3b and Figure 3c). For this reason, it is sometimes referred to as 2.5D X-ray microscopy, as it does not provide true 3D images. Laminography can be fast, yet only collection of full angular coverage scans as achieved by microCT or XRM can deliver isotropic 3D spatial resolution by having complete information for the tomographic image reconstruction [6].

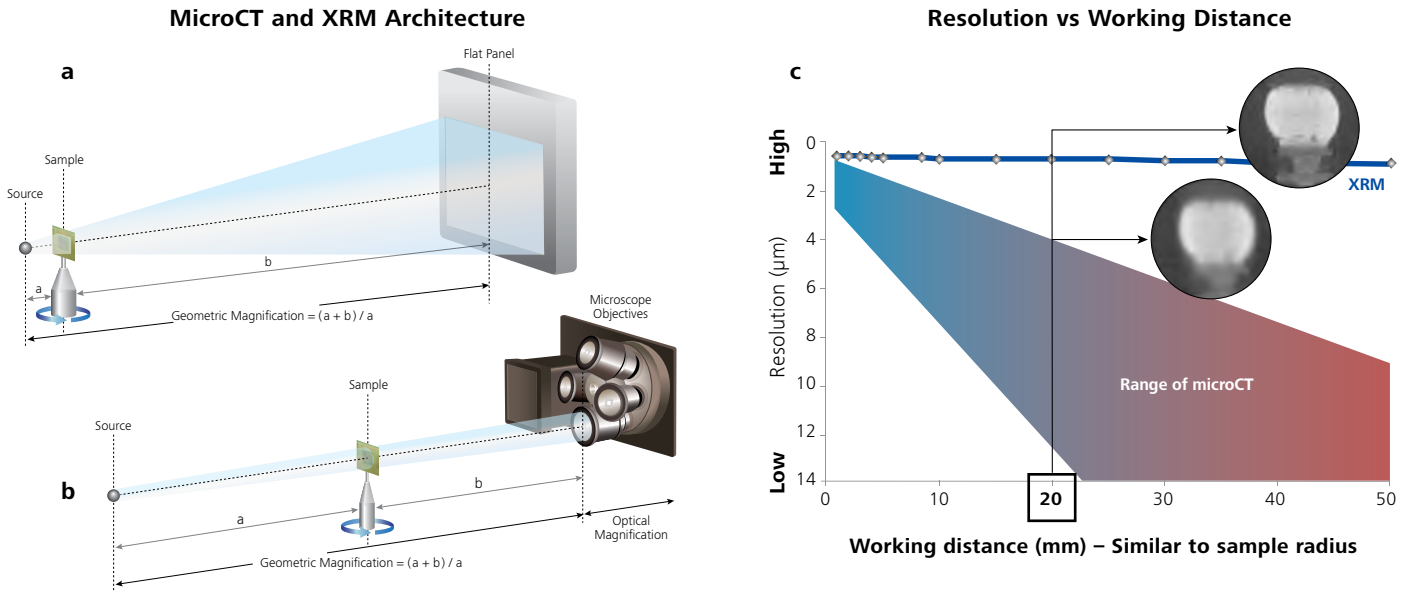

Figure 2 *a) The set-up for microCT imaging operates on principles of geometric magnification, b) 3D XRM implements optical magnification, c) XRM maintains high magnification at long working distances and high resolution for large samples.*

AI-Enabled 3D X-ray Microscopy

When 3D XRM emerged two decades ago it was a breakthrough method for non-destructive, high-resolution imaging of advanced packages, revealing details impossible to see in 2D X-ray projections (Figure 4). However, when imaging a region of interest (ROI) within a large sample at the highest resolution, 3D XRM throughput can be on the order of many hours. Additionally, like all microscopies, the high magnifications required for high resolution result in a small field of view. The combination of slow scan times and small field of view limits the volume of material that can be analyzed at high resolution. To address this, an artificial intelligence solution using deep learning high-resolution reconstruction algorithms (DLHRR) was recently introduced, enabling faster data acquisition, improved image quality, and faster overall FA workflows. It uses a convolutional neural network algorithm based on the "noise2noise" model [7], and a proprietary cost function and user-executed neural network training method using a small amount of data to train the neural network model. DLHRR enables scan time improvements by a factor of 4X to 10X across a broad array of sample types without sacrificing resolution or usability [8] and is available commercially as ZEISS DeepRecon Pro, a module for ZEISS X-ray microscopes.

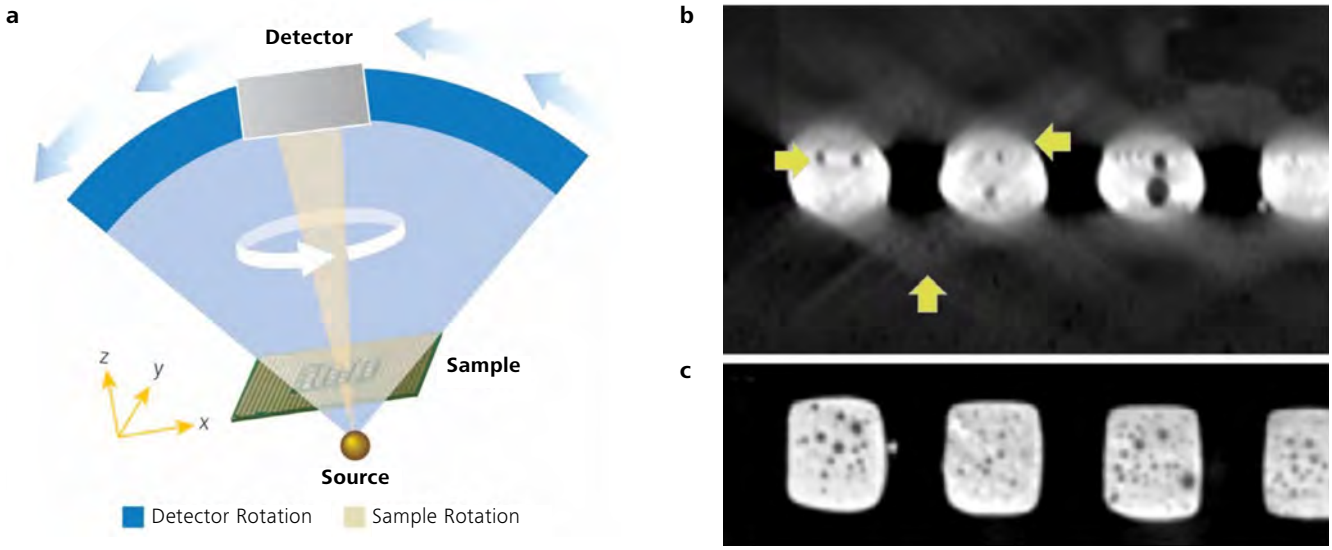

Figure 3 *a) Schematics of a 2.5D computed laminography setup, b) reconstructed XZ slice showing distorted structures and voids at the solder interfaces, and streak artifacts in the low-absorbing areas (arrows), c) reconstructed planar view XY.*

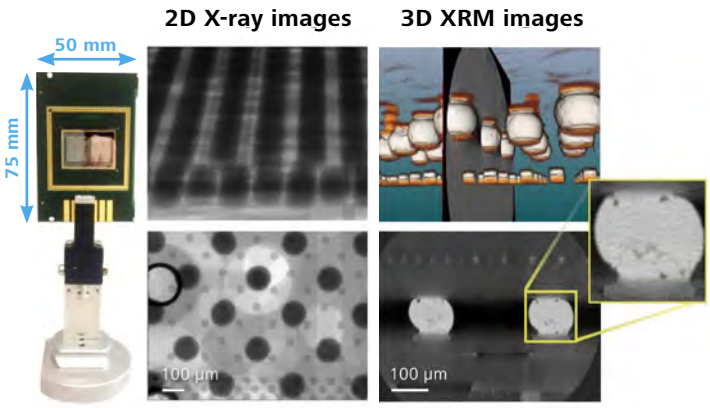

Figure 4 *3D XRM of a large 2.5D package reveals voids and cracks in flip chip bumps that are invisible in 2D X-ray images at any viewed angle.*

The speed gains come from the improved image contrast-to-noise ratios (CNR) that result from using DLHRR for 3D reconstruction instead of the common Feldkamp-Davis-Kreuss (FDK) or filtered back projection (FBP) algorithm, which uses a frequency domain filter. The high CNR enables a reduction in dwell time and/or the number of angular projections required for a high quality image (Figure 5a, to the right), and for semiconductor packages, the typical scan time improvement is 4X (Figure 6a).

To train the neural network model, a single XRM tomography data set is used. The trained network can be applied to other samples containing comparable X-ray attenuation and consistent scan parameters, including X-ray source and filter settings as well as magnification. Typically, no parameter tuning or customization by the operator is required. The training of a new network to address different scan settings or a new sample class takes about 3 hours, and the application of the network back to a reconstructed data set takes less than 5 minutes for a volume of 1000^3 voxels. This enables faster time to results for applications like construction analysis, FA and reliability studies where multiple similar parts must be scanned, and multi-site construction analysis, where multiple ROI in an individual sample are scanned with similar scan settings, such as for reverse engineering or fault isolation where stitching multiple fields of scan volumes is required. DLHRR is likely to benefit unique samples as well, due to the combination of faster scan speeds with relatively fast time for autonomous model training using an offline workstation. DLHRR can speed up high-resolution 3D XRM by using fewer X-ray projections to get results in a less time or can be used to improve the image quality by keeping scan time constant with a "full" projection data set. In some instances, both speed and better image quality are obtained simultaneously (Figure 6b and 6c). DLHRR's multisite stitching effectiveness was proven for a Bosch Sensortec accelerometer/gyroscope by creating a 3 x 3 array of nine fields of view, each covering a 4 mm x 4 mm area. The network model was trained using the FOV in the center of the array, and successfully applied to all eight others [9].

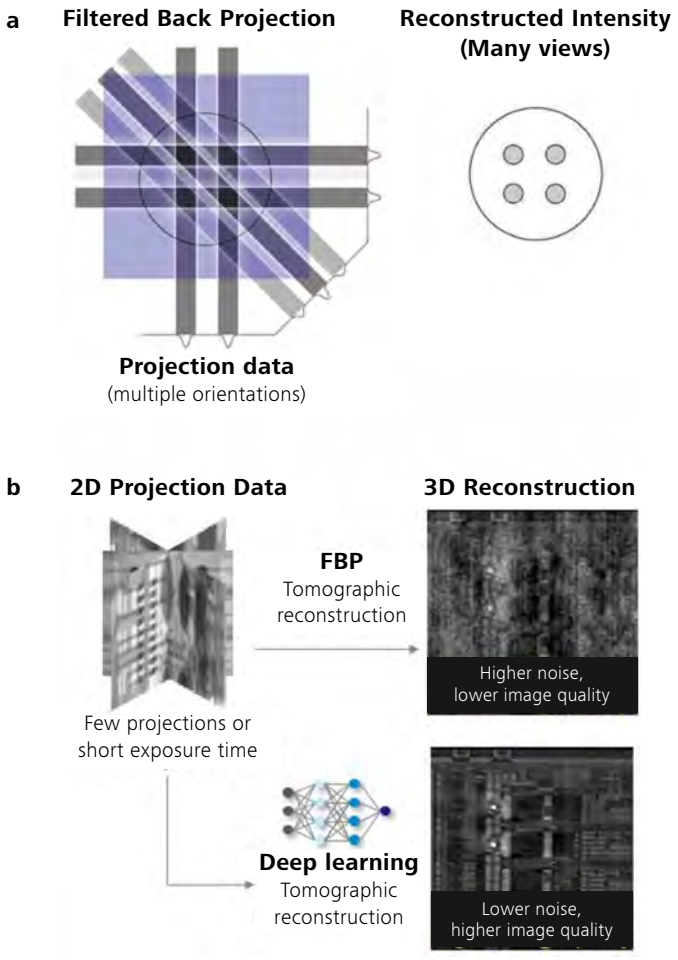

Figure 5 *a) In filtered back projection (FBP), projection data is filtered using a frequency domain filter, reducing image blurring. b) By integrating a pre-trained neural network between raw projection data and reconstructed data, high quality reconstructions can be achieved with low numbers of projections, and/or short exposures.*

The emergence of AI for 3D X-ray microscopy and package failure analysis enables more productive use of 3D XRM, higher FA success rates enabled by better image quality and improved CNR, and new applications that benefit from multiple-scan workflows on a single sample, or a single scan on multiple samples. Deep learning-based reconstruction decreases the effects of noise due to short exposure time and decreases the "streak" artifacts typically associated with sparse angular sampling. There are promising results for many types of samples, and the capability for a typical operator to easily train networks for new scan conditions or sample types will facilitate flexibility and responsiveness for a resource-constrained lab to adapt quickly to incoming requests. The application of AI to XRM makes the overall FA workflow faster, and it coincides with new innovations in FIB solutions addressing the physical failure analysis challenges of advanced packaging. Maximum benefit occurs when these advancements are combined into a synergistic workflow.

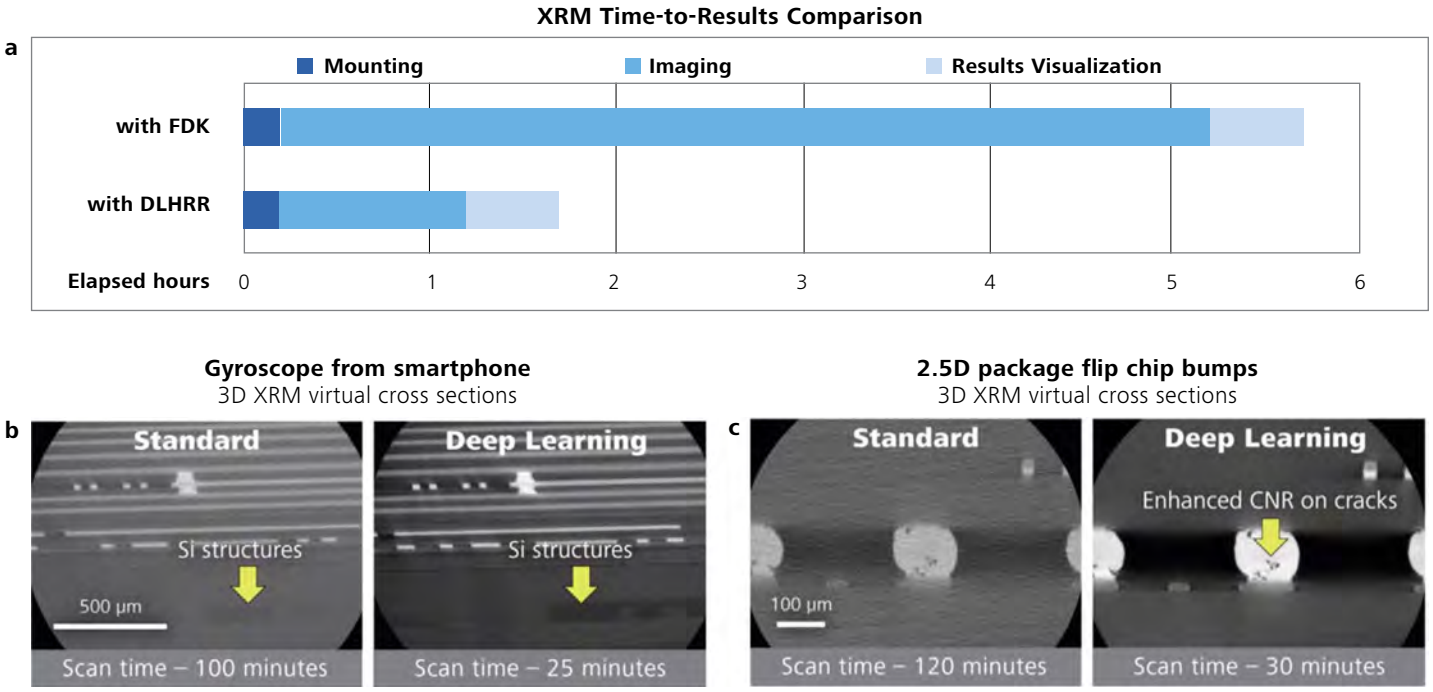

Figure 6 *a) DLHRR typically accelerates high-resolution 3D XRM imaging 4x versus using FDK reconstruction b) Image and scan time comparison for a gyroscope c) Image and scan time comparison for solder bumps in a large 2.5D large package.*

Advances in Focused Ion Beam Scanning Electron Microscopes

Drivers for New Cross Section Methods

According to the International Roadmap for Devices and Systems [10], near-term difficult packaging challenges include optimizing materials and processes for lower temperature assembly and for improved Cu resistance and reliability, while mitigating the impact of size effects in interconnect structures as they shrink. Meanwhile as packages become more complex, natural variations resulting from the packaging industry's historically wide process margins are emerging as a challenge for heterogenous integration, driving an increase in the volume of test die and learning cycles as failure modes are introduced through combinatorial package strategies [11]. This increased volume of test and learning cycles drives increasing pressure for fast and efficient analysis during development and later during production to maximize yields. Cross-sectional analysis is a common task in package construction evaluations and FA workflows. Cross sections allow one to view shapes and dimensions of interconnects, measure layer thicknesses, and check intermetallic quality, as well as study defects related to test, assembly and production process parameters, chip-package interactions, and thermomechanical stresses. Optically-guided cross sectioning of important package structures and features is becoming more difficult as 3D packaging implementing fine-pitch interconnect penetrates nearly every semiconductor business sector.

ROI are often deeply buried and with package interconnect pitches now crossing 1 µm, traditional mechanical cross sections are increasingly challenged to target features and accurately end-point to a desired sample plane with high success rates. Large-area and high-quality cross sections can be made using a BIB to fine polish mechanical cross sections, and it is possible to achieve a cross section through the full length of a 30 µm-diameter wirebond with application of best practices for such techniques [12]. However, the targeting accuracy limit for BIB is around 15 µm, which means it would be a challenge to consistently achieve cross sections in the center of today's 25 µm-diameter microbumps.

The milestone of 1 µm package interconnect pitch is driving the requirement for FIB-SEM analysis into the packaging world, ushering in a new cross section era mimicking that seen decades earlier for die-level semiconductor analysis. To extend the usefulness of FIB-SEM to package cross sections, a fs-laser has recently been integrated into the FIB-SEM. This enables rapid material removal on a scale of millimeters with micron levels of precision, followed by accurate fine polishing with nanometer levels of precision (Figure 7). Adopting an architecture where the laser is parallel to the e-beam, and laser processing occurs in a dedicated ablation chamber rather than in the high-vacuum imaging chamber, this "LaserFIB" is known commercially as ZEISS Crossbeam laser [13] and well suited for the shrinking structures defining this new era of packaging (Figure 8).

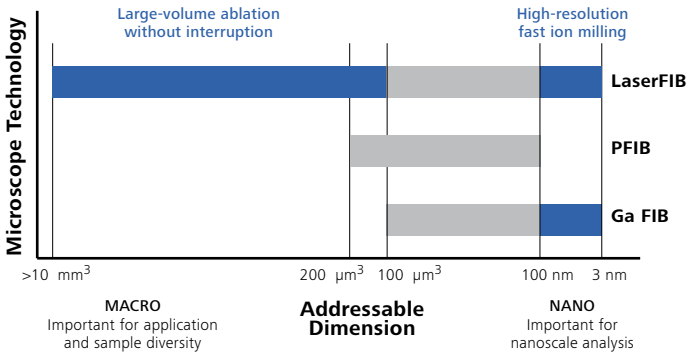

Figure 7 *A fs-laser integrated into a Ga FIB-SEM instrument enables rapid targeted removal of millimeter material volumes, enabling nanoscale imaging and analysis over large areas and from deeply buried sample locations.*

Laser-enabled Package Cross-Section Landscape

Standalone laser marking systems, even when using ps- or fs-lasers, lack integration and environmental conditions to efficiently target a small ROI by FIB after laser ablation. Commercial standalone laser systems implementing ultra-short-pulsed lasers specifically for sample preparation are effective for large-area preparation and package dissection but lack optimization for the fastest targeted microscopy preparation where ablation speed and sample quality are simultaneously important, since vacuum environments produce the best laser ablation and sample quality, in turn enabling efficiency for the subsequent FIB polishing steps. In contrast, the integrated LaserFIB approach has proven efficient and effective in correlative workflows with optical or XRM microscopy for a variety of research and industrial applications, including characterization of microbumps in a 3D package [14], development of automotive bumpers from recycled materials [15], correlative microscopy for rapid screening of Zr-containing particles for geochronology [16], and identification of random particles within an OLED display [17].

The combination of fs-laser integrated within a FIB-SEM using Ga beam technology has proven highly efficient. Since the fs-laser can be targeted with high accuracy to within microns of its target, with minimal redeposition and a laser-affected zone <1 µm, the remaining volume of material after optimized laser ablation is suitable to polish by FIB. Polishing requires lower currents than large-volume ion milling, and Ga beams have 10X higher current densities than plasma beams at these low currents (Figure 9). The combination of targeted fs-laser ablation with fast Ga beam polishing is so effective that it can outperform a standalone laser plus PFIB combination. As Figure 10 shows for the cross section case of a targeted 500 µm-diameter solder ball, the LaserFIB cycle time was half that of the standalone laser plus PFIB combination, resulting in a doubling of FIB capacity and 2X faster time to results. While results may vary across different applications, it demonstrates the LaserFIB integration effectiveness.

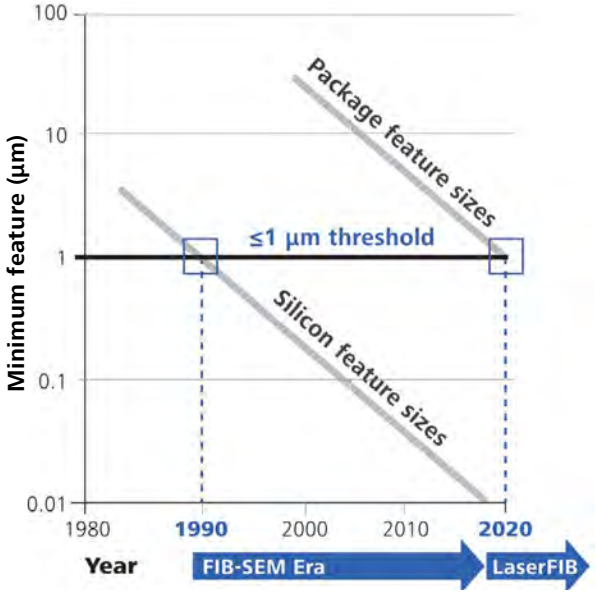

Figure 8 *As die-level features hit 1 µm dimensions in 1990, FIB-SEM became a required cross-section technique. Packaging features are now crossing that same 1 µm threshold, driving FIB integration with fs-lasers to enable efficient and targeted millimeter-wide package cross sections for nanoscale analysis of buried features. Graph inspired by [18].*

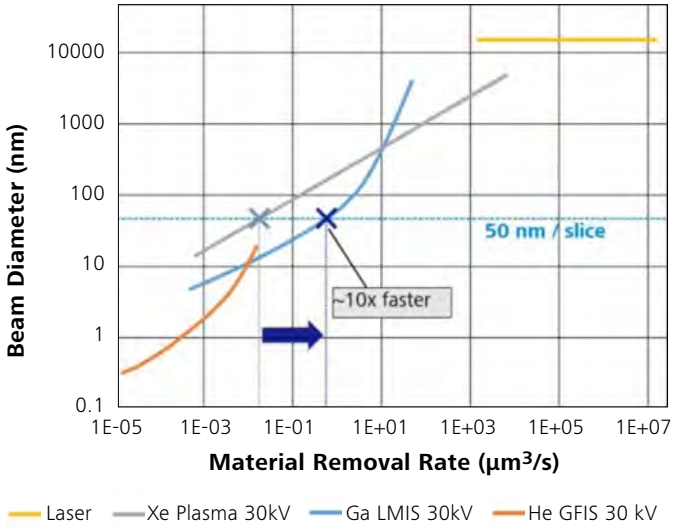

Figure 9 *Beam diameters plotted as a function of material removal rates show that a Ga FIB is 10X faster than a PFIB at typical "thin slice" conditions required for fine ion milling.*

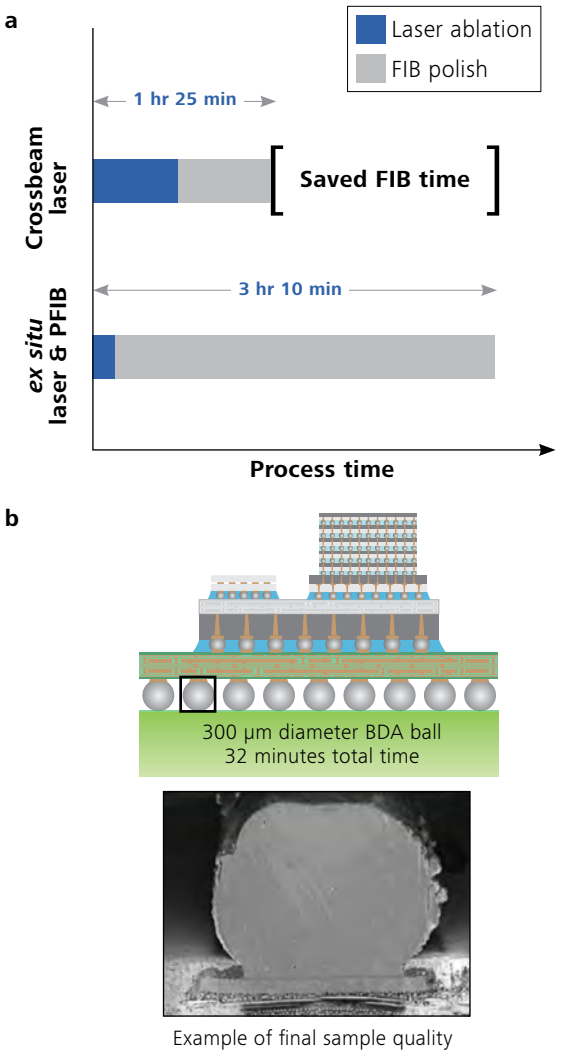

Figure 10 *a) A 500 µm-diameter solder ball was cross sectioned by the integrated LaserFIB and compared against a published workflow using a standalone laser and a PFIB [19]. The integrated LaserFIB saved FIB time and was 2X faster b) 32 minutes of LaserFIB preparation for a targeted 300 µm-diameter solder ball produces high sample quality.*

Due to the versatility enabled by a large laser scan area of 40 mm x 40 mm and an innovative cross-jet feature enabling the uninterrupted ablation of up to 10 cubic millimeters of material or more (depending on sample composition), the LaserFIB is suited for a broad range of different packaging and materials analysis applications, as indicated in Table 1 and Table 2.

Application	XRM correlation	Optical correlation
APU full cross section (15mm)		■
Buried Cu-pillar on GaAs die	■	
Bare wirebond ball bond		■
Seal ring on die		■
Solder ball cross section		■
SiC power module	■	
Unfilled TSV in GaN device		■
Trench-MOS with Cu clip	■	
Cu pillar solder bumps in IC	■	
Flip chip on board	■	
MEMS with metallic cap	■	
Multi-chip package	■	
Thermal interface material		■

Table 1 *Survey of correlative techniques in proven package FA LaserFIB cross section applications.*

Applications	Description	Suitability
2D laser cross sections	Remove volumes >> 2 mm^3 for large area imaging and analytics without breaking vacuum	■
Large-area EBSD	Prepare high-quality large surfaces for EBSD without ion polishing	■
TEM preparation	Efficiently and consistently prepare thin, site-specific, quality lamella for broadest range of materials including carbonaceous ones	■
Micromechanical test structures	Prepare large structures and large arrays in vacuum over a scan field of several centimeters, with unattended long running	■
Nanoscale XRM preparation	Create multiple sites (>0.5mm tall) anywhere from an intact large sample	■
Atom probe preparation	Prepare a large array of site-specific APT needles without using *in situ* lift-out	■
Correlated microscopy	Flexible, efficient sample-centric platform using features & fiducials on the sample for many modalities & length scales	■
TOF-SIMS	Air-free workflow to TOF-SIMS after laser cutting	■
No contamination	Main chamber kept free of laser-ablated debris	■
Avoidance of Ga-induced low-kV artifacts	Eliminate or minimize beam artifacts using milling, cryoFIB milling, or Ar polishing	■
Ga-free FIB polishing	Perform FIB milling without Ga	X
Fast viewing	Integrated SEM for efficient feedback of laser processing	■

Table 2 *LaserFIB suitability for different types of applications.*

The LaserFIB is well-suited as a site-specific cross section solution, where the ROI requires specificity better than 15 µm targeting accuracy, which is the limit for standard mechanical cross sectioning as discussed previously. Site specificity requires correlative microscopy, usually with X-ray or optical modalities. Computer aided design (CAD) layouts can also be helpful, but only 3D XRM reveals the true 3D location of buried objects. For the various applications listed in Table 1, slightly more than half involve buried features and require a 3D XRM correlative workflow to enable cross sectioning the designated site. Software solutions are available to aid the overlay of images of different modalities in the LaserFIB, including 3D XRM data. The laser spot's diameter is <15 µm, and with registration procedures, the laser's accuracy for targeting a surface feature can be better than 2 µm. The LaserFIB's Ga beam removes the excess material using live SEM imaging during FIB milling to achieve end-pointing in the targeted location, with accuracy better than 10 nm possible. The LaserFIB is also well-suited for tasks that have low targeting requirements, for example to prepare a sensitive interface or material that would fall apart using alternative methods. In general, laser ablation volumes should be kept in the range of 10 cubic millimeters or less, for reasons of time savings and ensuring uninterrupted laser operation.

Effective LaserFIB Workflows

As the technology moves into the field, new workflows are arising. A particularly effective LaserFIB workflow makes use of the fs-laser to create shallow "sample-centric" ruler-based surface fiducial marks for multimodal microscopy. The LaserFIB can laser scribe a T-shaped ruler to cover millimeters of area in less than a minute, with measurement divisions of 25 µm or more (Figure 11). The ruler is visible in optical, XRM, and SEM imaging modes, and adds efficiency to correlative workflows. In Figure 12 the ruler fiducials are used to guide the laser placement for site specific cross-sectioning of a targeted Cu pillar microbump in a smartphone package-on-package (POP). This example involved iterations of two-hour 3D XRM scans to aid process set-up and confirm target accuracy. In this case, the entire XRM to LaserFIB workflow took less than one day [17]. Figure 13 shows the steps of the workflow. The XRM scans are executed at steps A (for defect visualization) and E (to capture the fiducial marks by XRM). A third XRM scan (not shown) was performed right after laser ablation to confirm the proximity of the buried defect to the surface of the cut face. This was done as a precaution while developing the workflow and is an optional step.

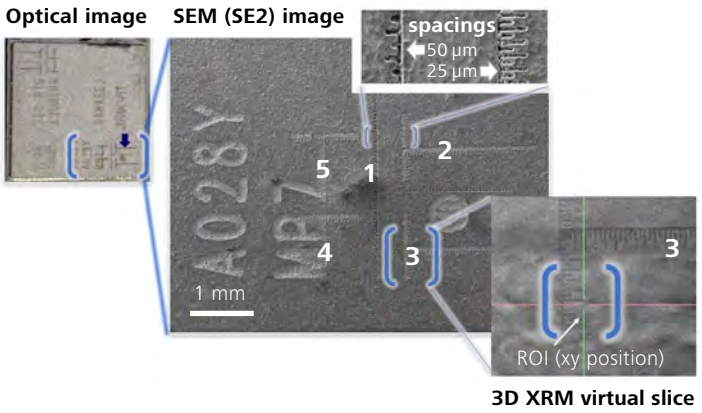

Figure 11 *Five shallow "T-shaped" ruler fiducials scribed onto the surface of a package-on-package sample are numbered for clarity. Ruler divisions are 25 and 50 µm (top image zoom). The XY position of the buried ROI relative to the fiducials is determined from a 3D XRM virtual slice at the sample's surface (right image zoom).*

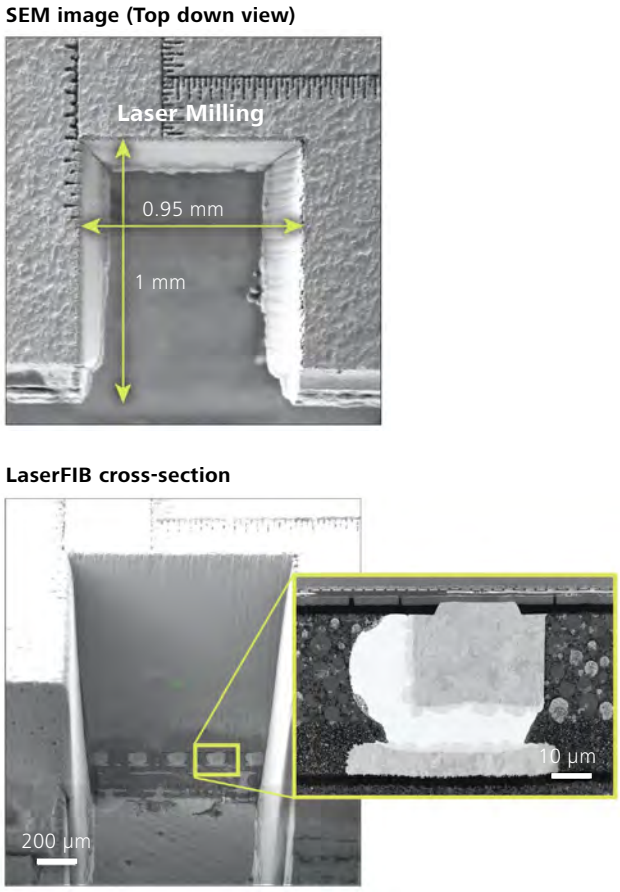

Figure 12 *A small Cu-pillar bump in a smartphone package-on-package (POP) is accurately targeted, cross sectioned and imaged with the aid of laser-made fiducials.*

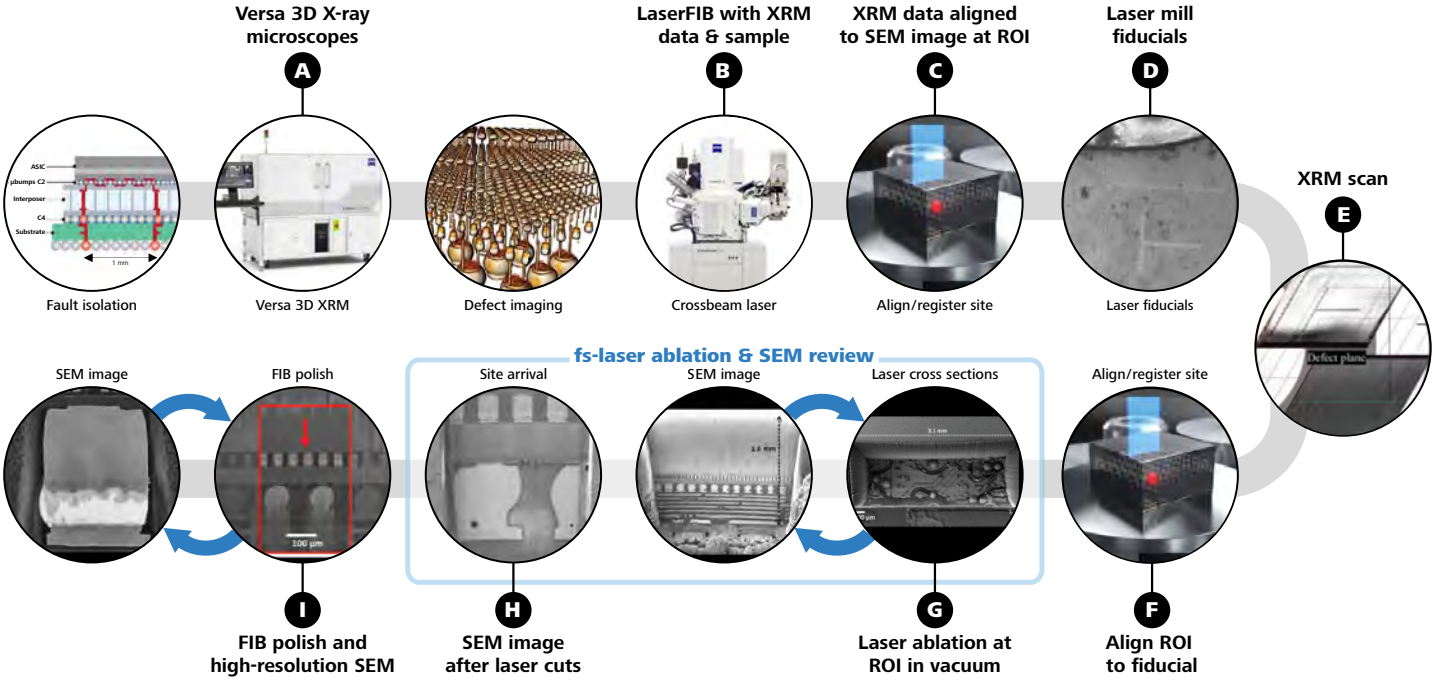

Figure 13 *Steps of a correlative XRM to LaserFIB workflow. Sample-centric "ruler" fiducials are created at step D, scanned in XRM, and then visualized in the LaserFIB to guide the targeted ablation. The rulers can also be created as the first step. Integration facilitates iterative cut and view cycles (solid box) for laser optimization and end-pointing.*

Summary

The inspection and analysis of 3D packages is becoming more difficult due to buried package interconnects that have higher I/O densities and finer pitches, the insufficiency of 2D analysis, and the increase in cycle time as the package complexity and volume of testing increase. Rapid and precise analysis of deeply buried structures is essential. Advancements in 3D X-ray microscopy and FIB-SEM microscopes offer significant speed improvements. In an AI-enabled approach to improve faster data acquisition, 3D XRM has incorporated deep learning algorithms. Meanwhile, the FIB-SEM has been integrated with a fs-laser, resulting in the LaserFIB, a new class of FIB-SEM instrument. As a result, 3D XRM data acquisition speeds can be increased by 4X and sometimes more than 10X, while the LaserFIB enables millimeters of material removal within minutes to hours, instead of the days required by conventional Ga or plasma FIB. With these new 3D XRM and FIB-SEM advancements combined into an optimized correlative workflow, it is possible to produce high-resolution microscopy images enabled by the FIB's submicron targeting precision and the fs-laser's rapid material removal, which provides access to deeply buried features with submicron laser-affected zones. These advancements enable multi-site sampling at practical timescales and extend the toolset for package development, failure analysis and reliability studies. This supports fast development of reliable next-generation package technology by enabling the combination of speed, site targeting, and end-pointing accuracy required to address increasingly complex devices with higher throughput and success rates.

Acknowledgments

The authors wish to thank the many people in the ZEISS demonstration centers around the world that developed the first applications with these new instruments, as well as ZEISS colleagues Stephan Hiller and Ravi Sanapala for being stalwart champions in guiding the new product developments.

References

[1] ASE Group, What is 2.5D? [Video], https://ase.aseglobal.com/en/technology/advanced_25dic (2022) Accessed on July 16, 2022 at https://coms.aseglobal.com/marcom/video/25d-ic at timestamp 1:20.

[2] A. Gupta, Z. Tao, D. Radisic, H. Mertens, O. V. Pedreira, S. Demuynck, J. Bömmels, K. Devriendt, N. Heylen, S. Wang, K. Kenis, L. Teugels, F. Sebaai, C. Lorant, N. Jourdan, B. Chan, S. Subramanian, F. Schleicher, A. Peter, N. Rassoul, Y. Siew, B. Briggs, D. Zhou, E. Rosseel, E. Capogreco, G. Mannaert, A. Sepúlveda, E. Dupuy, K. Vandersmissen, B. Chehab, G. Murdoch, E. Altamirano Sanchez, S. Biesemans, Z. Tőkei, E. D. Litta and N. Horiguchi, Buried power rail integration for CMOS scaling beyond the 3 nm node, SPIE (2022).

[3] H. S. P. Wong, K. Akarvardar, D. Antoniadis, J. Bokor, C. Hu, T.-J. King-Liu, S. Mitra, J. D. Plummer and S. Salahuddin, Proceedings of the IEEE, 108, 478 (2020).

[4] C. D. Hartfield, T. M. Moore and S. Brand, in Microelectronics Failure Analysis: Desk Reference, 7th ed., T. Gandhi Editor, ASM International (2019).

[5] B. A. J. Quesson, P. L. M. J. v. Neer, M. S. Tamer, K. Hatakeyama, M. H. v. Es, M. C. J. M. v. Riel and D. Piras, in Proc.SPIE (2022).

[6] A. Gu, M. Terada and A. Andreyev, A Brief Comparison of Computed Laminography versus 3D X-ray Microscopy for Electronics Failure Analysis, Carl Zeiss Microscopy GmbH [White Paper], (2022).

[7] J. Lehtinen, J. Munkberg, J. Hasselgren, S. Laine, T. Karras, M. Aittala and T. Aila, Noise2Noise: Learning Image Restoration without Clean Data, in Proceedings of the 35th International Conference on Machine Learning, D. Jennifer and K. Andreas Editors, p. 2965, PMLR, Proceedings of Machine Learning Research (2018).

[8] M. Andrew, R. Sanapala, A. Andreyev, H. Bale and C. Hartfield, Supercharging X-ray microscopy using advanced algorithms, in Microscopy and Analysis, Wiley Analytical Science (2020).

[9] A. Gu, A. Andreyev, M. Terada, B. Zee, S. Mohammad-Zulkifli and Y. Yang, in ISTFA 2021, p. 291 (2021).

[10] IEEE, The International Roadmap For Devices and Systems: 2021, [White Paper], (2021).

[11] E. Sperling, Variation Making Trouble In Advanced Packages, in Semiconductor Engineering, [White Paper], (2022).

[12] T. Rodgers, A. Gu, G. Johnson, M. Terada, V. Viswanathan, M. Phaneuf, J. de Fourestier, E. Ruttan, S. McCracken, S. Costello, A. M. Robinson, A. Gibson and A. Balfour, in ISTFA, p. in press (2022).

[13] B. Tordoff, C. Hartfield, A. J. Holwell, S. Hiller, M. Kaestner, S. Kelly, J. Lee, S. Müller, F. Perez-Willard, T. Volkenandt, R. White and T. Rodgers, Applied Microscopy, 50, 24 (2020).

[14] M. Kaestner, S. Mueller, T. Gregorich, C. Hartfield, C. Nolen and I. Schulmeyer, in CSTIC, China (2019).

[15] T. Schubert, R. Salzer, A. Albrecht, J. Schaufler and T. Bernthaler, Combined light-microscope – FIB/SEM failure analysis on automotive body parts, [White Paper], (2021).

[16] J.H. Li, Q.L. Li, L. Zhao, J.H. Zhang, X. Tang, L.X. Gu, Q. Guo, H.X. Ma, Q. Zhou, Y. Liu, P.Y. Liu, H. Qiu, G. Li, L. Gu, S. Guo, C.-L. Li, X.H. Li, F.Y. Wu and Y.X. Pan, Geoscience Frontiers, 13 (2022).

[17] V. Viswanathan, L. Jiao and C. Hartfield, in 2021 IEEE 23rd Electronics Packaging Technology Conference (EPTC), p. 80 (2021).

[18] R. Hollman, in Pan Pacific Microelectronics Symposium (2019).

[19] M. Tuček, R. Blando, R. Váňa, L. Hladík and J. V. Oboňa, in International Physics of Failure Analysis (IPFA), Singapore (2020).

microscopy@zeiss.com
www.zeiss.com/semiconductor-microscopy